IEEE Access
Multidisciplinary | Rapid Review | Open Access Journal

Received 30 June 2022, accepted 27 July 2022, date of publication 5 August 2022, date of current version 11 August 2022.

Digital Object Identifier 10.1109/ACCESS.2022.3196779

RESEARCH ARTICLE

Impacts of Large-Scale Offshore Wind Power Plants Integration on Turkish Power System

YUNUS YALMAN[1], ÖZGÜR ÇELIK[2], ADNAN TAN[3], KAMIL ÇAĞATAY BAYINDIR[1], ÜMIT ÇETINKAYA[4], MERDEN YEŞIL[4], MEVLÜT AKDENIZ[4], GIBRAN DAVID AGUNDIS TINAJERO[5], (Member, IEEE), SANJAY K. CHAUDHARY[5], (Senior Member, IEEE), JOSEP M. GUERRERO[5], (Fellow, IEEE), AND BASEEM KHAN[6], (Senior Member, IEEE)

[1]Department of Electrical and Electronics Engineering, Ankara Yildirim Beyazit University, 06010 Ankara, Turkey
[2]Department of Energy Systems Engineering, Adana Alparslan Turkes Science and Technology University, 01250 Adana, Turkey
[3]Department of Electrical and Electronics Engineering, Cukurova University, 01250 Adana, Turkey
[4]Turkish Electricity Transmission Corporation (TEIAS), 06520 Ankara, Turkey
[5]Department of Energy Technology, Aalborg University, 9100 Aalborg, Denmark
[6]Department of Electrical and Computer Engineering, Hawassa University, Hawassa 1530, Ethiopia

Corresponding author: Baseem Khan (baseem.khan04@gmail.com)

This work was supported in part by the Offshore Wind Farms Large-Scale Integration in Turkey—WindFlag Project (www.windflag.et.aau.dk) funded by the Danish International Development Agency (DANIDA) Fellowship Centre and the Ministry of Foreign Affairs of Denmark to Conduct Research in Growth and Transition Countries under Grant 19-M03-AAU and in part by the Scientific and Technological Research Council of Turkey International Research Fellowship Program for Ph.D. Students under Grant BIDEB-2214-A.

ABSTRACT In this paper, the impacts of large-scale OWPPs penetration on the Turkish power system are addressed. The grid compliance analyses for the large-scale OWPP integration are carried out by using the grid connection criteria defined in the Turkish grid code. PV and QV curves are obtained to assess the effect of OWPP on the static voltage stability limit. Eight scenarios are conducted to analyze the effect of the OWPP on the static and dynamic characteristics of the power grid. To observe the large-scale OWPP impact on the voltage and frequency stability, transient events such as the outage of conventional power plants and three-phase to ground faults are applied. The results of the voltage and frequency stability analysis reveal that the Turkish grid remains stable after the integration of an 1800 MW OWPP. Furthermore, the Turkish system remains stable even in the event of an outage of the international transmission lines to Bulgaria and Greece.

INDEX TERMS Grid code, grid integration, offshore wind power plants, voltage/frequency stability.

NOMENCLATURE

DFIG	Doubly Fed Induction Generator.
ENTSO − E	European Network of Transmission System Operators for Electricity.
FRT	Fault-Ride Through.
HVRT	High Voltage Ride-Through.
LVRT	Low Voltage Ride-Through.
NREL	National Renewable Energy Laboratory.
OHLs	Overhead Lines.
OWPPs	Offshore Wind Power Plants.
PCC	Point of Common Coupling.
PV	Active Power-Voltage.
PQ	Active and Reactive Power.
RE	Renewable Energy.
RESs	Renewable Energy Sources.
TEIAS	Turkish Electricity Transmission Corporation.
TSO	Transmission System Operator.
QV	Reactive Power-Voltage.
WPPs	Wind Power Plants.
WT	Wind Turbine.
ROCOF	Rate of change of frequency.

The associate editor coordinating the review of this manuscript and approving it for publication was Giambattista Gruosso.

I. INTRODUCTION

The use of renewable energy sources (RESs) is continuously increasing worldwide due to several factors, including the depletion of fossil fuels, energy security, and increasing environmental concerns. Wind and solar power plants are the prominent RESs with an installed capacity of 743 GW and 760 GW, respectively, as of 2021 [1]. The European Union aims to achieve at least 32% renewable energy (RE) penetration level by 2030, while Denmark looks forward to approximately 55% RE penetration level by 2030 and 100% by 2050 [2]–[4]. Likewise, Massachusetts, New Jersey, and Washington DC have pledged the RE penetration of 55% by 2050, 50% by 2030, and 100% by 2032, respectively [5].

The grid code published by the Energy Market Regulator Authority and the Ministry of Energy and Natural Resources in Turkey defines the grid connection criteria for wind and photovoltaic power plants [8]. during the preliminary planning and design stages, simulation studies must have been carried out to confirm that the renewable power plants meet the grid connection criteria.

Several authors have analyzed the effect of RES integration in different countries [7]–[23]. In [7], the impact of large-scale photovoltaic generation systems on Egypt's national grid has been investigated and The maximum allowable generation from proposed RES for different regions is determined considering line congestion. In [8], with the integration of a new WPP (517 MW) into the Egyptian grid, the voltage stability performance of the grid in case of a three-phase short circuit is investigated. In [9], the effect of dynamic characteristics of a photovoltaic power plant on the short-term voltage stability of the transmission system is examined in case of severe voltage sag. In [10], dynamic voltage stability analysis has been performed to check whether low voltage ride-through (LVRT) and high voltage ride-through (HVRT) requirements are achieved for a three-phase short circuit in the Northern Jordanian power system with a large-scale photovoltaic energy system. The results show that Static Var Compensation is required to satisfy VRT requirements in some cases. In [15]–[19], the static voltage stability of power grid is evaluated using PV curve method. In [16], the effects of large-scale photovoltaic generation on the Bangladesh power system have been examined in terms of voltage, frequency, and angle stability. In [17], the static and dynamic performance of the Moroccan southern power grid with large-scale WPP is investigated. The dynamic analysis has been performed to observe power system behavior in case of a three-phase fault at the critical connection busbar. The results show that the Moroccan power system does not face any stability problems with integration of renewable power plants. In [18], the static and dynamic impact of the large-scale renewable energy systems on the Lesotho power grid is investigated. Voltage, frequency, and rotor angle are observed by applying a short circuit at the critical busbar in dynamic analysis. Static voltage analysis has been performed according to the hourly load of 2018. The results demonstrated that an increased penetration level of RES causes grid instability. In [19], the effect of a large-scale distributed Photovoltaic generation system on the Ontario power grid has been investigated in terms of voltage and frequency stability according to penetration level. In [20], the impact of a large-scale photovoltaic wind generation system on the voltage and frequency stability of Jordan's power grid has been examined in steady-state and contingency situations, such as short circuits and outages of the main power plant. In [21], dynamic and static voltage stability analyses are performed for the Tunisian national grid with large-scale renewable generation comprised of 14 different photovoltaic power plants with a total power of 937 MW. In [22], the effect of a large-scale renewable generation system on the Moroccan national grid has been investigated by performing power flow calculations and contingency analysis for the various case studies. The results show that voltage regulation devices are required due to the variability of wind power. The impact of 120 MW WPP on the power grid within the Southwest Power Pool in the United States has been discussed in [23].

The studies presented in this paper are a part of the Offshore Wind Farm Large-Scale Integration project in Turkey (WindFlag) [24]. This project identified a potential of 1.8 GW OWPP in two phases at the Kiyiköy site located in the Black Sea region [25]. The main objective of this paper is to examine the impact of the OWPP integration into the Turkish national grid. The whole Turkish grid and OWPP models are implemented using DıgSILENT PowerFactory 2021. The operational performance of the power system is tested using actual data provided by TEIAS.

The main contributions of the present research can be summarized as follows:

- The detailed grid code compliance analyses are presented to confirm that the designed large-scale OWPP meets grid code requirements.
- The scenarios are carried out to analyze the static and dynamic characteristics of the power grid. The increase in the static stability limit of the power grid in presence of OWPPs is determined.
- Voltage stability limits of the Turkish power grid are estimated using the PV and QV curves.
- To the best of the author's knowledge, no work related to the impacts of large-scale OWPP on the Turkish power network has been documented in the literature.
- This work features the analysis of the network reliability, capacity, and limits characterizations by using the real network data taken from the TSO. High capacity reserve type electricity generation plants are geographically concentrated in specific regions; hence this study presents a power system constraint for the Turkish power system by ensuring power flow characteristics.

This paper is organized as follows: In Section II, the National grid of Turkey is introduced. The status of wind energy in Turkey is presented in section III. In section IV, the system under study is explained. The grid compliance

study of large-scale OWPP according to grid code is given in section V. Voltage and frequency stability analysis of the Turkish power grid including the large-scale OWPP is performed in different case studies in section VI. Finally, Section VII provides the conclusions of this work and future works are mentioned.

II. TURKISH POWER SYSTEM DESCRIPTION

The Turkish transmission system consists of 400 kV and 154 kV voltage levels. Since September 2010, Turkey's electric grid has been synchronized with the ENTSO-E via 400 kV transmission lines to Bulgaria (two lines) and Greece (one line). There are also various 400 kV interconnections with neighboring countries Syria, Iran, Iraq, and Georgia. At the end of November 2021, the total electric power consumption of Turkey reached 300.6 TWh. According to the electricity consumption statistics for 2020, the annual electricity consumption of Istanbul was 38.5 TWh, while the annual consumption in other big cities in the Marmara region was 33.4 TWh [27]. As shown in Fig. 1, the total electricity generation was mostly dependent upon imported fossil fuels like coal and natural gas, while the RES provided only around 15% of the electricity generation [27]–[28].

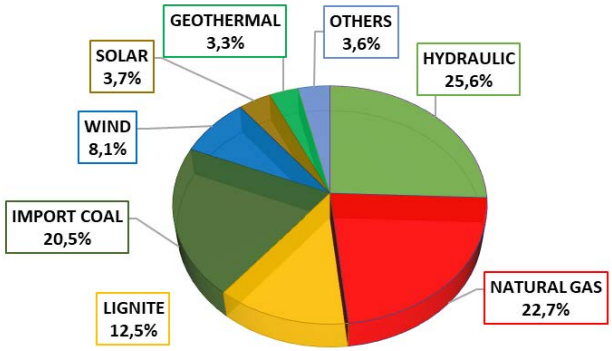

FIGURE 1. Energy production by Resources at the end of 2020 in Turkey.

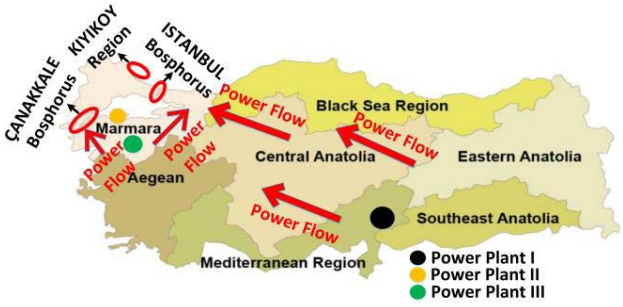

FIGURE 2. Description of general power flow of Turkish grid.

The location of the three most important power plants (I, II, and III) and the general load flow direction in the Turkish power system are shown in Fig. 2. [29]. The power generation capacity of the West Anatolian (southwest of the Marmara region) region is higher than its consumption. Thus, the surplus electric power generation from the west Anatolian region is exported through the Çanakkale Bosphorus to the Trakya region (the north of the Marmara region) using the 400 kV submarine cables.

Turkey had 77.9 TWh hydropower generation capacity in 2020 and most of these plants are in the eastern and southeastern Anatolia regions [30]. As the consumption in these regions is less than the production, the surplus energy flows to the western part of Turkey. This specific situation can create severe conditions, like inter-area oscillation and rotor angle stability problems if there are contingencies like faults or power plant outages. In this context, rotor angles of large power plants in the eastern and western sides of Turkey need to be observed during stability analyses. Power grid constraints for voltage and frequency are given in Table 1 and Table 2, respectively.

TABLE 1. Voltage limit values for transmission system.

Voltage level (kV)	Normal operation		Contingency Disconnect	
	Min	Max	Min	Max
400	340	420	-	450
154	140	170	-	-

TABLE 2. Frequency limit values for transmission system.

Operating frequency (Hz)	Time
47.5-48	10 min
48-48.5	20 min
48.5-49	1 hour
49-50.5	permanent
50.5-51.5	1hour

III. WIND ENERGY STATUS IN TURKEY

The cumulative installed wind power capacity in Turkey is 9305 MW and additionally 1872 MW is under construction. All these WPPs are onshore. Turkey has 75 GW offshore wind power capacity [31]; however, there is not any offshore project. This situation shows that the development of the offshore wind sector can contribute to reaching the 50% renewable energy target of Turkey [32].

Due to the average wind speed above 7 m/s, the Aegean, Marmara, and Eastern Mediterranean regions are attractive for wind farm developers [33]. Kıyıköy is considered a candidate area for connecting large-scale OWPP as the average wind is greater than 8.75 m/s and it meets other criteria such as low water depth and free from military zones and shipping routes [25].

IV. SYSTEM UNDER STUDY

A. SYSTEM DESCRIPTION

Kıyıköy OWPP is proposed for the development of 900 MW in phase I and 900 MW in phase II. Kıyıköy Phase-I will be connected to Substation-A with 400 kV double circuit overhead lines (OHL), and Kıyıköy Phase-II is connected to BUS A and BUS B with a single 400 kV OHLs as shown in Fig.3.

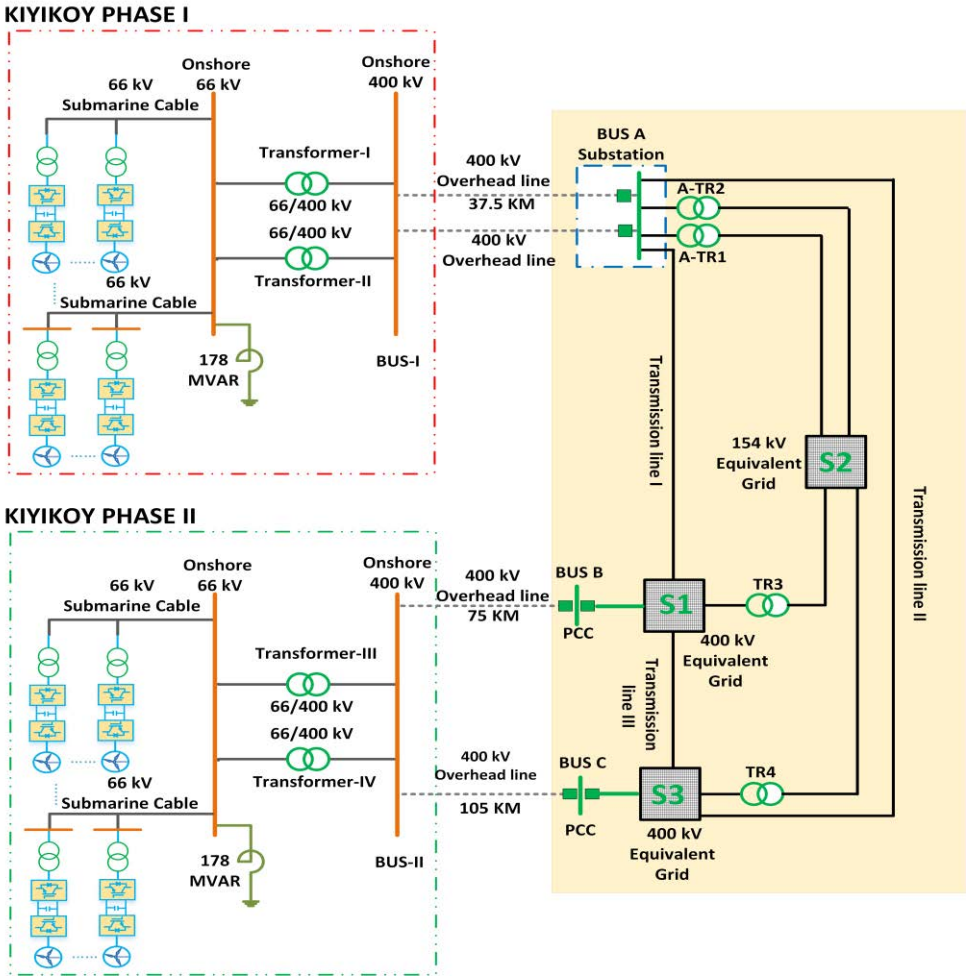

FIGURE 3. Basic representation of the system under study.

Each OWPP stage has 60 units of 15 MW WT units which are based on NREL's model [34]. Additionally, there are 178 MVAr shunt reactors to compensate reactive power generated by the submarine cable feeders. A single-line diagram of the OWPPs and equivalent grid model is given in Fig. 3. The parameters of the equivalent model are given in Table 3. The capacity of specified generation plants related to the case studies is given in Table 4. The full model of the Turkish grid was used in the simulation, even though a simplified Single line diagram is shown here for the sake of clarity.

Turkey has a large power grid consisting of 2034 synchronous machines, 5294 busbars, and 4772 transformers. The total installed capacity, substation, and transmission line length of the Turkish power grid are 99.38 GW [35]. All stability analyses are performed for the complete Turkish power grid.

B. POWER PLANT AND WT CONTROLLER

The block diagram of WT controllers is given in Fig. 4 [36]. The power plant controller has been modeled using the station controller model and the WT controllers have been implemented using the full-scale WT converter controller model of DıgSILENT PowerFactory software [36]. The ratings of the converters used in the WTs are given in Table 5.

The WT controller has 4 components as described in [36]:

- **Reactive and active power (PQ) controller:** It generates current references for the current controller located in the inner loop. The active control loop generates the d-axis current reference and the reactive power control loop generates the q-axis current reference for the current controller. The PQ controller contains additional control blocks to supply fault ride-through (FRT). If the grid voltage is detected out of limits, the WT provides reactive power support to the grid.
- **The current controller** contains two PI controllers for d-axis and q-axis current control loops and it generates voltage references to the grid side converter of the Model.
- **Active power reduction controller**responds to frequency deviation in the grid and it generates an active power reduction factor for the PQ controller.

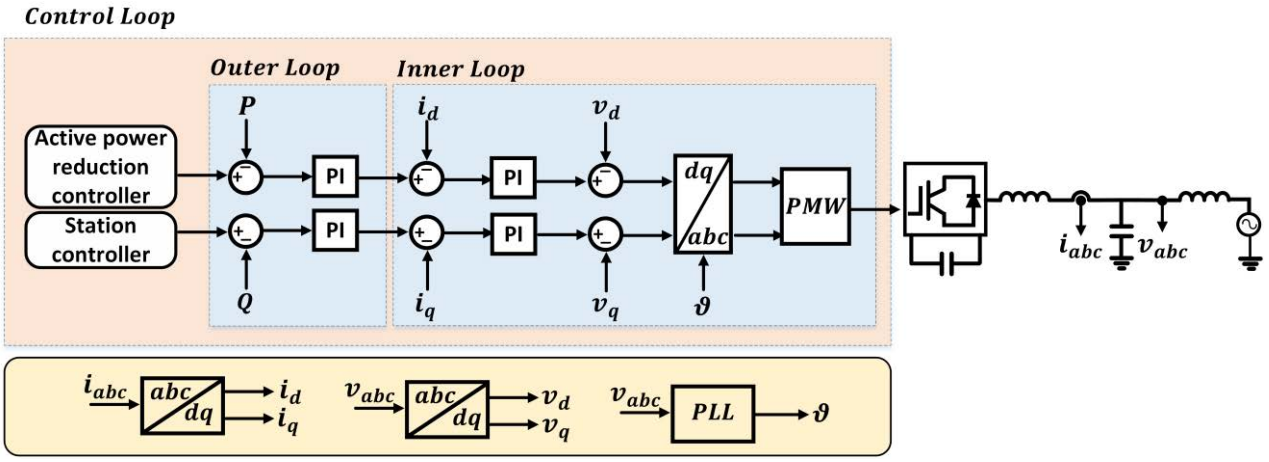

FIGURE 4. Simplified diagram of WT and power plant controller.

TABLE 3. Data of equivalent grid under study.

Transformer	ATR-1	ATR-2	TR-3	TR-4
Power (MVA)	250	250	100	100
Voltage Level (kV)	400/154	400/154	400/154	400/154
U_k	12%	12%	11.36%	34.36%
Location	**S1**	**S2**	**S3**	
Short circuit power (MVA)	4670	1128	5211	
Short circuit current (kA)	6.74	4.22	7.52	
X/R	13.4	7.4	15.3	
Transmission line	**Length**	**X/R**	**Charging power MVAr/100km**	**X**
Transmission line I	38	12.7	69	265 mΩ\km
Transmission line II	90	12.7	69	265 mΩ\km
Transmission Line III (coupling effect)	-	12	0	52 Ω

TABLE 4. Capacity of some generation plants.

Plant	Power MVA
Power plant I	315
Power plant II	360
Power Plant III (PP III)	775

TABLE 5. Converter ratings.

Parameter	Value
Voltage (kV)	3.3
Power (MVA)	16,7
Power Factor	0,9
Interfacing reactor impedance (Ω)	1,1314

- **Station controller:** The station controller of OWPP performs voltage or reactive power control at the PCC according to the grid code requirements. In the simulation studies, the control modes of station controllers have been selected as voltage control modes for both of the OWPPs at BUS A, B, and C which are considered as the PCCs. The reactive power control has a droop of 4% according to the grid code.

The WT controllers' parameters used in the simulation studies are given in the Appendix. The WT controller parameters are determined considering the grid code requirements.

V. GRID CODE COMPLIANCE ANALYSIS

The grid code compliance studies are performed to confirm that the planned Kıyıköy Phase-I OWPP complies with the grid code. The studies are categorized into four parts:

i Reactive power capability test;
ii LVRT test;
iii Voltage control test; and
iv Frequency response test.

A. REACTIVE POWER CAPABILITY TEST

The grid code defines the required WPP reactive power capability curve as demonstrated in Fig. 5 with a blue line. The result of the reactive power capability test is shown in Fig. 5 with the red curve. As the wind park can be operated at all points inside the red polygon, it can be concluded that the OWPP fulfills reactive power capability requirements.

B. LVRT TEST

The requirements of LVRT outlined in the grid code are illustrated in Fig. 6. During the period that the PCC phase-to-phase voltage remains in zones 1 and 2, the power plant must remain connected to the grid in case of voltage drops in one or all phases. Otherwise, the power plant is expected to be disconnected from the power grid.

The system FRT-mode response is tested by applying the three-phase short circuit to the PCC for 200 ms and the voltage at the PCC goes down to 0% as shown in Fig 7. The post-fault oscillations are well-damped WTs provide 1 pu

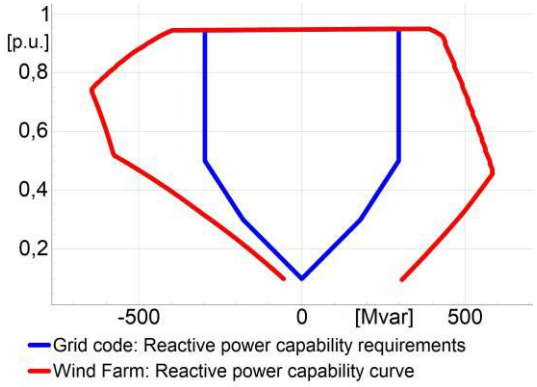

FIGURE 5. Reactive power capability curve of OWPP (red line), reactive power capability requirements of grid code (blue line).

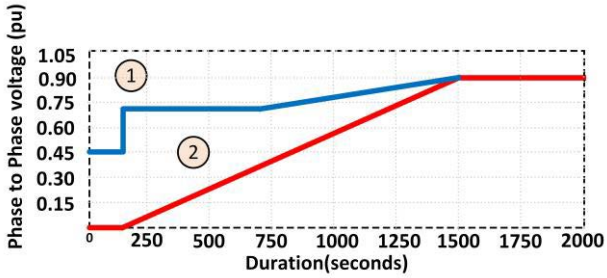

FIGURE 6. LVRT capability required by the grid code.

reactive current during the fault as per the requirement. It can be concluded that the turbine's reactive current injection rate reaches 100% of the nominal value in 30 ms. According to the grid code, the turbine is expected to reach the maximum reactive current, which is stated as up to 100% of the nominal current, in 60 ms with a 10% tolerance. Fig. 8 shows converter voltage and current during the three-phase to ground fault. It converter remains connected to the grid and it provides the reactive current to support PCC voltage during the fault.

This confirms that the OWPP remains connected to the power system in case of severe fault and provides reactive current to support the grid voltage. Thus, the OWPP satisfies LVRT grid code requirements.

C. VOLTAGE CONTROL TEST

Reactive power support from the OWPP depends on the droop value which is defined as the ratio of the p.u. change in voltage to the p.u. change in reactive power produced by the WT. Mathematically, it can be written as,

$$\text{Droop}(\%) = \frac{\Delta U / U_{nom}}{\Delta Q / Qmax} \tag{1}$$

According to TEIAS (Transmission system operator), it can vary between 2% and 7% range, though the value is generally set at 4%. The droop value is calculated using (1).

The reactive power support requirements in the WPP based on the grid code are shown in Fig. 9., the power plant should start to respond in 200 ms, and the reactive output power

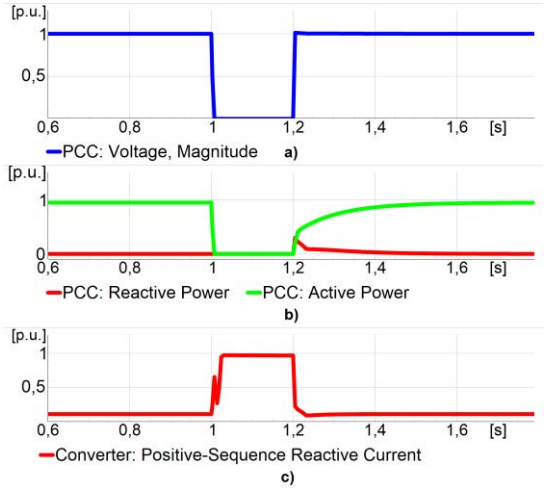

FIGURE 7. %100 penetration level; LVRT simulation results, (a) PCC voltage; (b) OWPP active and reactive power (c) positive sequence reactive current of WT.

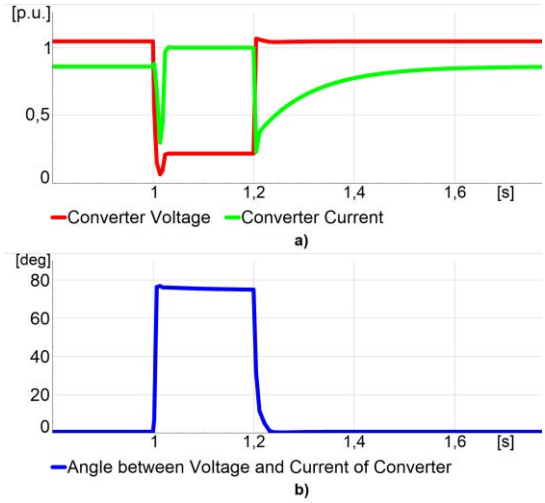

FIGURE 8. LVRT simulation results, (a) Converter voltage and current; (b) Converter phase angle.

should reach 90% of the nominal value within 1 second and stabilize within 2 seconds. The peak value of the oscillations that may occur in the reactive output power should not exceed 2% of the actual change.

The voltage step changes of 5% magnitude are applied to the PCC in order to check the reactive power response from the OWPP and the results are shown in Fig. 10. The plant response time starts within 20 ms against t. This response time is determined as at least 200 ms in the grid code [13]. On the other hand, the plant reactive power response it reaches the nominal balance value in 300 ms. In the grid code, the injected reactive power is expected to balance completely in 2 seconds. Thus, reactive power requirements are achieved well within the time periods stipulated in the grid code.

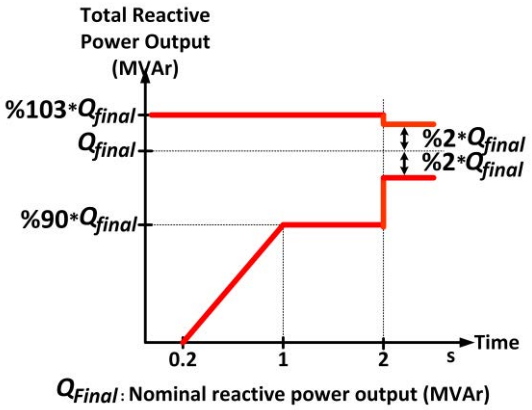

FIGURE 9. Reactive power support requirements of WPP based on grid code.

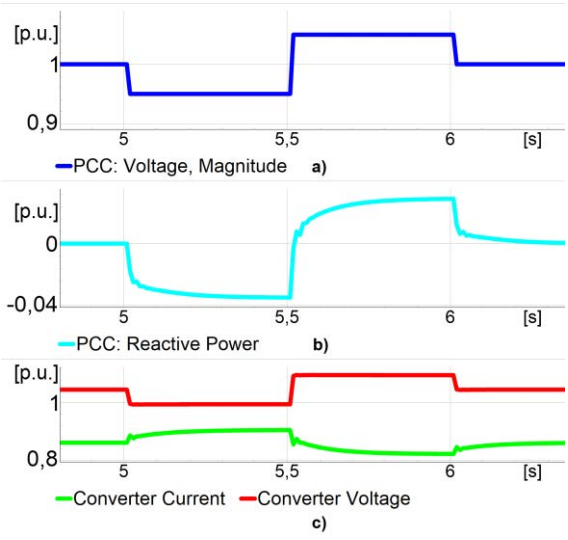

FIGURE 10. 100% penetration level (a) Bus voltage set-point variation in time; (b), Reactive power variation in voltage test simulation with 4% droop; (c) Converter current and voltage.

D. FREQUENCY RESPONSE TEST

The frequency response requirement of the grid code is shown in Fig. 11. The WPPs are expected to operate at full power capacity between 47.5 Hz and 50.3 Hz. when the grid frequency exceeds 50.3 Hz, the power is to be reduced at the rate of 0.5 pu/Hz of the excess frequency till 51.5 Hz.

An equivalent voltage source is connected at the PCC and its frequency is varied stepwise for analyzing the power reduction response of the WPP and the results are given in Fig. 12.

When the grid frequency is increased to 51 Hz, the active power output of the OWPP decreases from 1 p.u. to 0.7 p.u. as per the requirement of 0.5pu/Hz. When the frequency reaches 51.5 Hz, the active power output of the OWPP drops to zero. Thus, gird code frequency response requirements are satisfied by the planned OWPP.

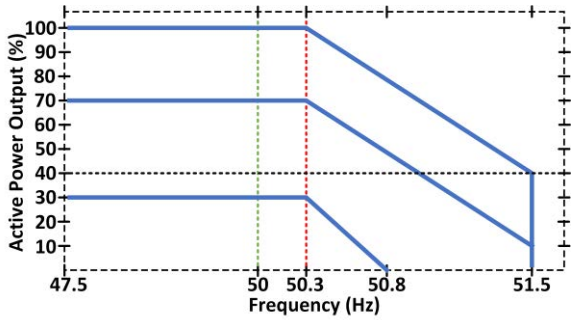

FIGURE 11. The required frequency response curve of WPP by the grid code.

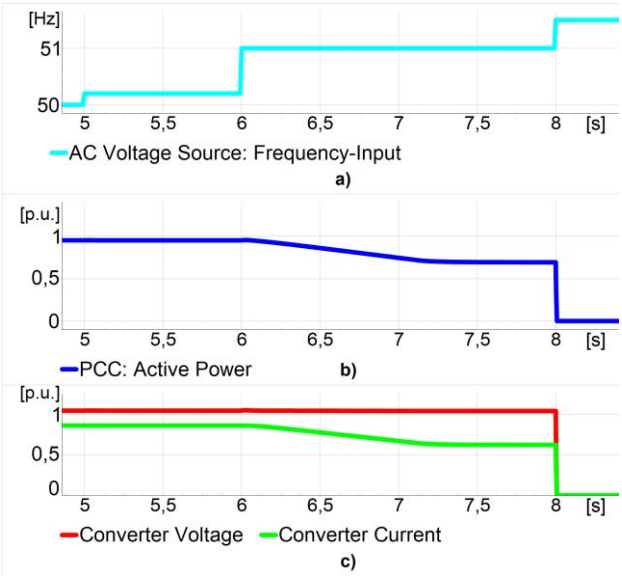

FIGURE 12. 100% penetration level (a) The applied frequency step change of the grid at frequency test case; (b) Frequency test result with 100% active power; (c) Converter current and voltage.

As can be seen from the test results, the proposed OWPP satisfies all grid code requirements. During the test, it is observed that the controller parameters should be properly adjusted to meet the grid code requirements.

VI. VOLTAGE AND FREQUENCY STABILITY ANALYSIS

Voltage and frequency stability are two electrical power quality critical parameters that define the power system performance. A series of simulation studies are performed using the complete model of the Turkish power grid including the planned large-scale OWPP to examine the Turkish power system voltage and frequency stability including RES.

A. STATIC VOLTAGE STABILITY ANALYSIS

Voltage stability is the capability of the power system to maintain acceptable bus voltages at every node under normal operating conditions. Increasing the load demand or changing the system conditions causes a gradual voltage drop, which can lead to an unmanageable voltage drop during a fault

condition, hence provoking voltage instability problems in the power system. The main reason for voltage instability is usually a lack of reactive power support, weak grid strength due to contingencies, or very high overload conditions in the power system [37].

Active power vs. voltage (PV) and Reactive power vs. voltage (QV) curves are used to determine the critical active and reactive power limits for steady-state voltage stability limits. To investigate the Turkish power system steady-state voltage stability, PV and QV curves are obtained for some of the critical busbars in the system and at the PCC of the OWPP.

(i) PV Curves: The PV curves of BUS K (the most critical bus in the power system) and BUS C (connection point to the OWPP with the main grid) are shown in Fig. 13 and Fig. 14, respectively. The PV curves of other connection points are not shown since the voltage control in BUS B is provided by the synchronous generator. Moreover, as BUS A is a strong bus, the voltage level of BUS A remains almost nominal. Voltage profiles of the OWPP connection point and critical bus are illustrated in Fig. 13 and Fig. 14. For each bus, three voltage profile curves are acquired: (i) without OWPPs, (ii) with the OWPP providing active power at the unity power factor, and (iii) OWPP providing both the active power and voltage regulation at the PCC. These curves show that the critical load level increases from 50970 MW to 51775 MW when the OWPP is connected. Moreover, when the OWPP voltage control is activated, it increases to 51845 MW.

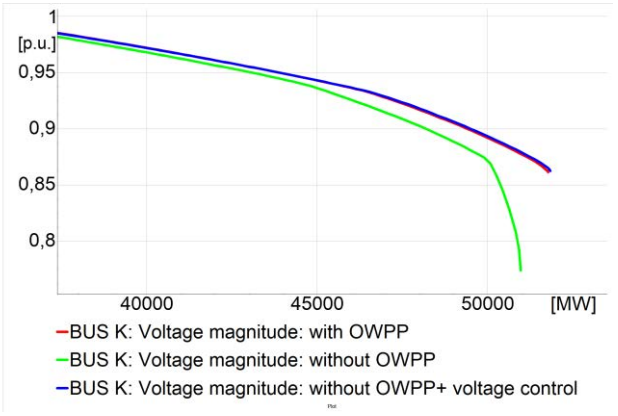

FIGURE 13. PV curve at the critical bus, -bus K.

(ii) QV curves: The QV curves of BUS K and BUS C are shown in Fig. 15 and Fig. 16, respectively. The substation steady-state voltage profiles are depicted for different cases., the critical reactive power levels of Bus K and BUS C are summarized in Table 7. As shown in Fig.16, the maximum reactive power level for BUS C increases from 1300 MVAr to 2960 MVAR when the OWPP is connected. Moreover, when the OWPP voltage control is activated, it increases to 3200 MVAr. Since the critical reactive power is much higher than the operating point of the power grid, it does not pose a problem in terms of steady-state voltage stability.

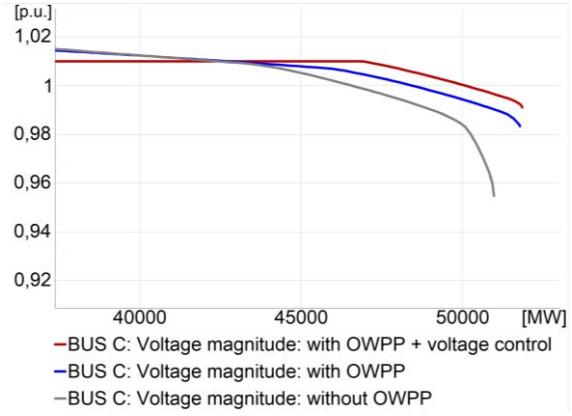

FIGURE 14. PV curve of the connection point of Phase-II OWPP.

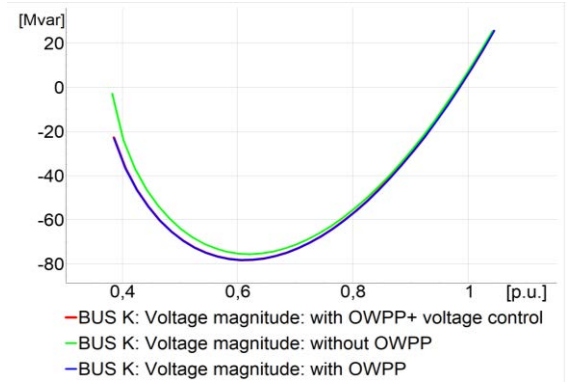

FIGURE 15. QV curve at the critical bus, Bus K.

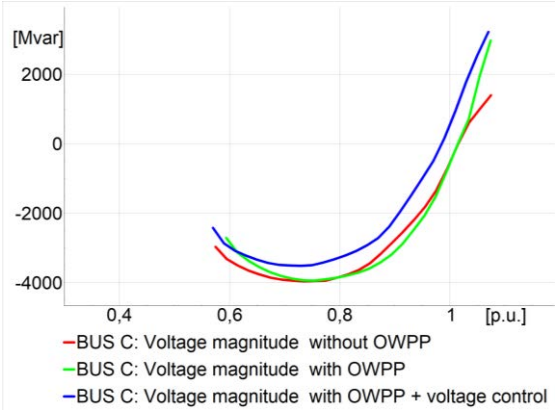

FIGURE 16. QV curve at the connection point of Phase-II OWPP.

The OWPP increases the stability limit at both the buses, and it is better when the voltage regulation is activated.

B. DYNAMIC VOLTAGE STABILITY ANALYSIS

The dynamic voltage stability analysis has been investigated by evaluating the busbar voltages during the three-phase to ground faults at some of the most critical buses determined by the TEIAS. The fault cases are listed below:

TABLE 6. Critical voltage level for different case studies.

	Without OWPP		With OWPP		With OWPP+ voltage control	
	BUS K	BUS C	BUS K	BUS C	BUS K	BUS C
Critical voltage Level (p.u.)	0.62	0.73	0.60	0.75	0.60	0.73
Reactive power level (MVAr)	-75	-3951	-79	-3934	-78	-3057

i A three-phase to ground fault has been applied to 400 kV buses at the PP III bus for 100 ms, and
ii A three-phase to ground fault has been applied to the 400 kV Transmission line I for 120 ms, which is the most critical transmission line outage for the Turkish power system
iii A three-phase to a ground fault has been applied to the proposed OWPP busbar for 100 ms.

The voltage dynamics at the faulted busbar and nearby busbars are investigated in detail. In addition, frequency variations and rotor angle variations are examined to see the response of the power grid in the case of simulated fault events.

1) THREE-PHASE SHORT CIRCUIT AT 400 kV BUSBAR OF PP III

A three-phase to ground fault is applied at the 400 kV PP III bus at the instant of 40 s. In Fig. 17, the voltage variations at the faulted busbar and the nearby busbar during fault are demonstrated. While the voltage level at the faulted busbar is zero as shown in Figure 17 with a blue line, the voltage level of the nearby busbar changes according to the distance between the fault point and the busbar. After fault clearing, the voltage of the Turkish power system attains nominal voltage levels in 40.32 s.

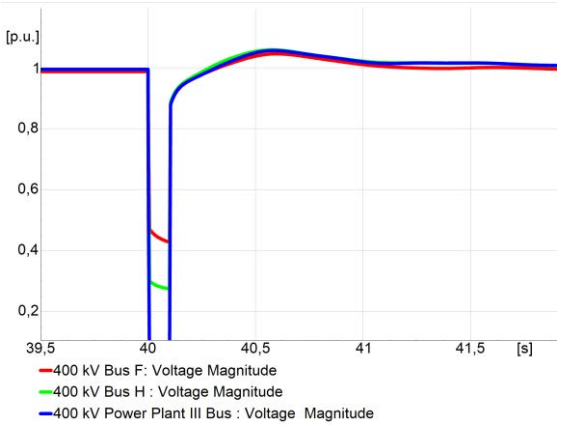

FIGURE 17. Voltage variation at 400 kV busbar of PP III and nearby substations during a three-phase ground fault.

Fig. 18 (a) presents the frequency of Bus A, and Fig. 18(b) shows the rotor angle of power plant I and power plant II.

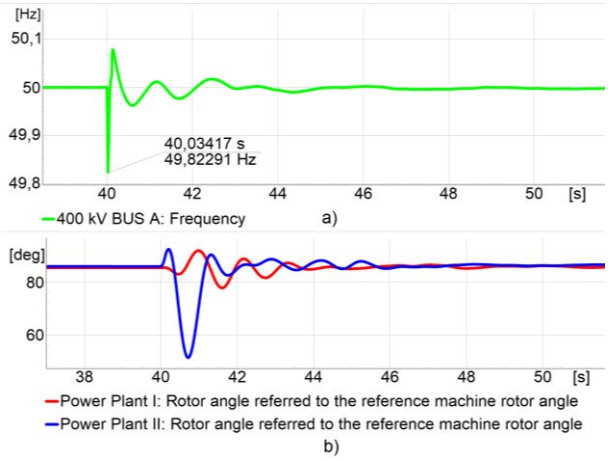

FIGURE 18. Frequency response of power system b) The rotor angle response of generators.

When the fault happens, the PP III is disabled and the frequency of the power system begins to decrease until the 49.82 Hz (frequency nadir). On the other hand, oscillation is observed in the rotor angles of important generators. After the fault clearing, frequency is restored and rotor angle oscillation in is damped within 5 s.

During the fault, the active power of the OWPP Phase -I decreased, and it provides 0.08 pu reactive current to support the voltage recovery as shown in Fig. 19. After fault clearance, the active power and reactive power of OWPP reach the nominal value again.

2) THREE-PHASE SHORT CIRCUIT AT 400KV TRANSMISSION LINE I

A three-phase to ground fault is applied at 400 kV Transmission Line I at the instant of 40 s and the resultant voltage variations at the selected buses are shown in Fig. 20. The fault is applied at 30% of the transmission line length. The voltage level at the line ends falls down to 0.2 and 0.25 p.u. during the fault. They recover to the nominal value within 100 ms after fault clearance.

The frequency is restored and rotor angle oscillation of the power plants I and II decay within 9 s after fault clearance as shown in Fig 21. The reduction of the active power of and injection of the positive sequence reactive current from OWPP Phase-I during the fault is shown in Fig 22.

3) THREE-PHASE SHORT CIRCUIT AT 400KV BUS A

A three-phase to ground fault is applied to the 400 kV BUS at the instant of 40 s and the resultant voltage variation is shown in Fig. 23 for the cases with and without the OWPP After clearing the fault, the voltage recovery time of BUS A is shown in Fig. 23.

It can be observed that the reactive currents injected by OWPP Phase-I and Phase-II assist to support the voltage levels at the faulted bus, and the OWPPs remain connected to the grid despite the zero voltage level.

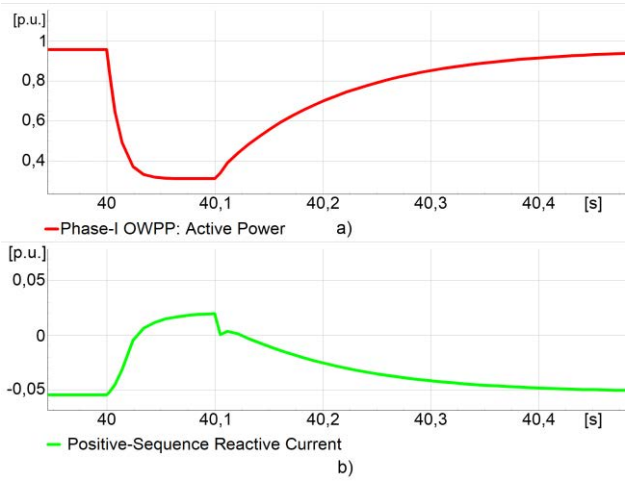

FIGURE 19. (a) Active power of Phase-I OWPP; (b) Positive sequence reactive current.

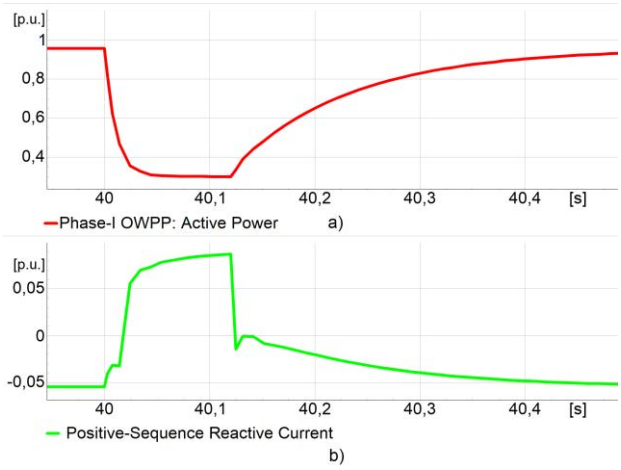

FIGURE 22. (a) Active power of Phase-I OWPP; (b) Positive sequence reactive current.

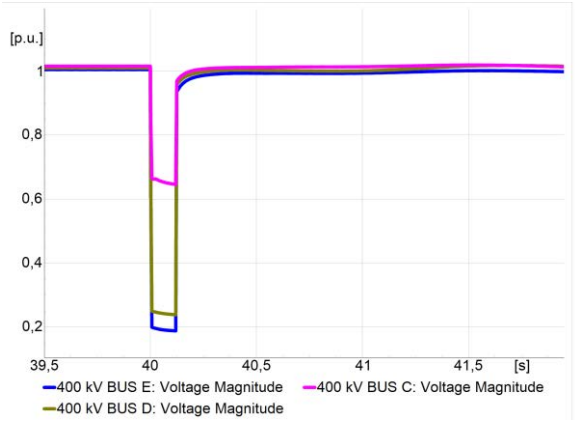

FIGURE 20. Voltage variation at transmission line busbar and nearby substations during a three-phase ground fault.

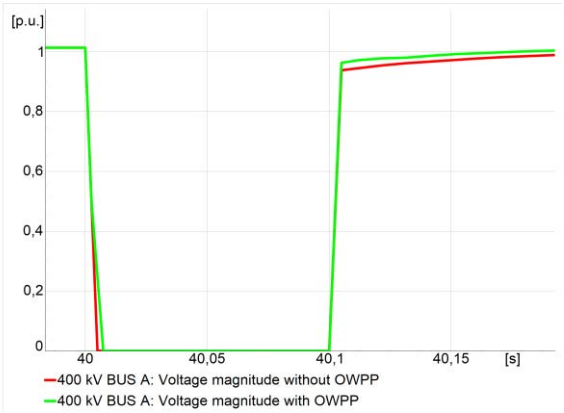

FIGURE 23. Voltage variation at busbar during the three-phase ground fault without and with OWPP.

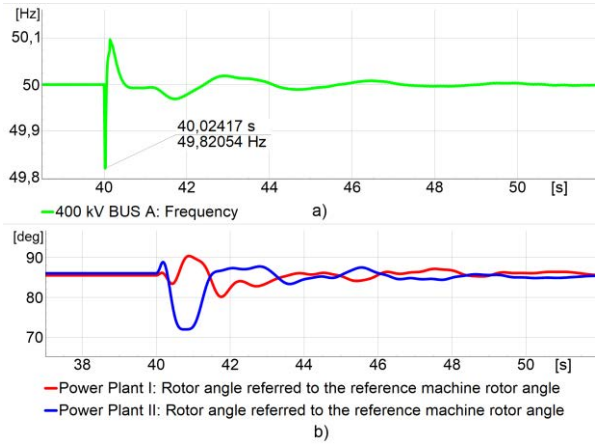

FIGURE 21. a) Frequency response of power system b) The rotor angle response of generators.

C. FREQUENCY STABILITY ANALYSIS

In this case, the frequency stability of the Turkish grid is examined through the simulation of different under full or zero power operations of the OWPP. The OWPP is said to be at full power if it is generating the rated output power. Likewise, if it is said to be at zero power, if it is not generating any power. The OWPPs were replaced with conventional power plants in frequency stability studies.

The scenarios are listed below:

- Case study I: Outage of PP III with the OWPP at zero power;
- Case study II: Outage of PP III with the OWPP at full power;
- Case study III: Outage of PP III with the OWPP at zero power and without interconnection line to other countries;
- Case study IV: Outage of PP III with the OWPP at full power and without interconnection line to other countries;
- Case study V: Adding new load with the OWPP at full power and without interconnection line to other countries;

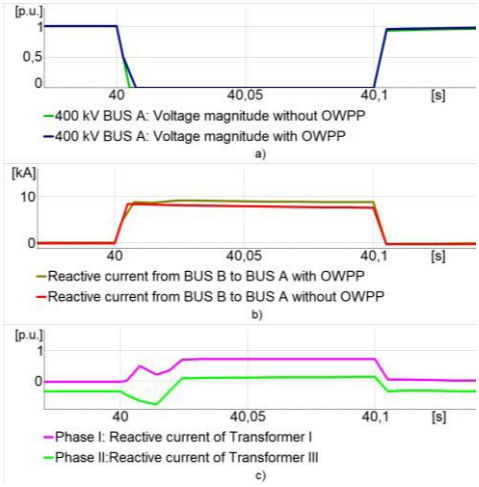

FIGURE 24. a) Voltage variation at BUS A during the three-phase ground fault; b) Reactive current from BUS B to BUS A c) Reactive current from OWPPs.

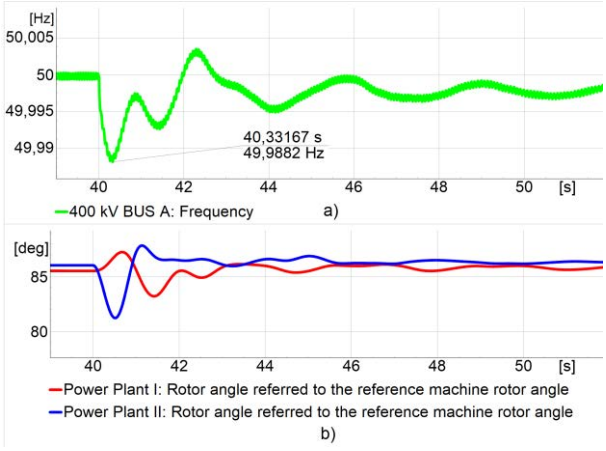

FIGURE 25. a) Frequency response of power system b) The rotor angle response of generators.

- Case study VI: Outage of PP III with the OWPP at full power and without interconnection line to other countries considering grid forming controller

1) OUTAGE OF PP III WITH OWPP AT ZERO POWER

PP III is tripped at the instant of 40 s to examine the frequency stability for OWPP at zero power and the results are shown in Fig. 25. Due to the outage of PP-III, the system frequency begins to decrease until the nadir is 49.982 Hz. The oscillations are observed in the rotor angles of the important generators and the oscillation decay within 10 s. Case study-I is determined to observe the effect of OWPP integration on frequency stability. The results are compared with case study-II.

2) OUTAGE OF PP III WITH THE OWPP AT FULL POWER

PP III is disabled to examine the frequency stability for OWPP at full power at the instant of 40 s. The results of the outage are shown in Fig. 26. Fig. 26 (a) demonstrates the frequency variation of the Turkish power system after an outage of PP III. Fig. 26 (b) illustrates the rotor angle response of critical generators. As can be seen in Fig. 26, the system frequency begins to decrease until the nadir is 49.987 Hz. Moreover, the results show that the frequency and rotor angle of critical generating plants are stable after tripping of PP III with an OWPP at full power

According to the penetration level, traditional power plants are disabled when the OWPPs are integrated into the power system. Therefore, the total power system inertia decreases. This affects the frequency response of the power system. When we compare the frequency nadir value for zero power and full power OWPP, the frequency nadir is higher at zero power OWPP.

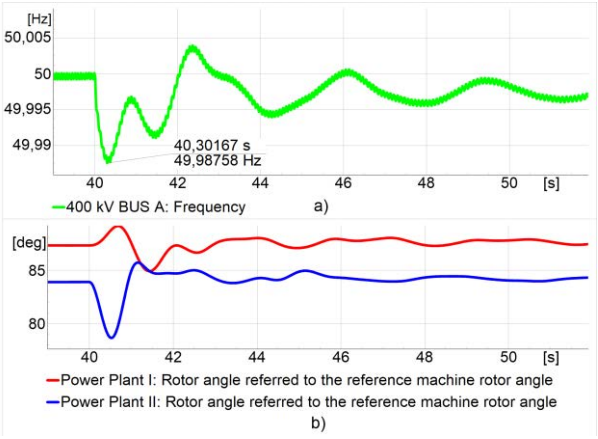

FIGURE 26. a) Frequency variation of power system b) The rotor angle response of generators.

3) OUTAGE OF PP III WITH OWPP AT ZERO POWER AND WITHOUT INTERCONNECTION LINE TO OTHER COUNTRIES

PP III is disabled to examine the frequency stability for OWPP at zero power without interconnection line to other countries at the instant of 40 s. The results of the outage are shown in Fig. 27. Fig. 27 (a) illustrates the frequency response of the Turkish power system after an outage of a critical conventional power plant when the interconnection line to other countries has opened. Fig. 27 (b) shows the rotor angle response of important generators. As can be seen from the results, the system frequency begins to decrease until the nadir is 49.76 Hz. The frequency of the Turkish power system without interconnection line deteriorates more as compared to the interconnected operation mode (case study-I) at zero power OWPP. However, the frequency has remained stable because of the availability of the spinning reserve.

4) OUTAGE OF PP III WITH OWPP AT FULL POWER AND WITHOUT INTERCONNECTION LINE TO OTHER COUNTRIES

PP III is disabled to examine the frequency stability for OWPP at full power without interconnection lines to other

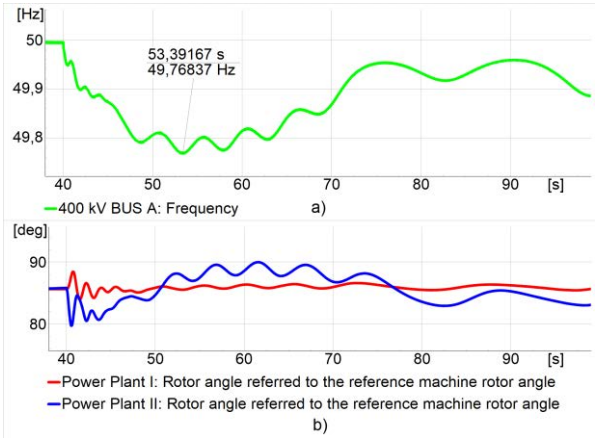

FIGURE 27. a) Frequency variation of power system b) The rotor angle response of generators.

countries at the instant of 40 s. The results of the outage are shown in Fig. 28. Fig. 28 (a) shows the Turkish power system frequency variation after an outage of a critical conventional power plant with OWPP at full power without interconnection. Fig. 28 (b) shows the rotor angle response of critical generators.

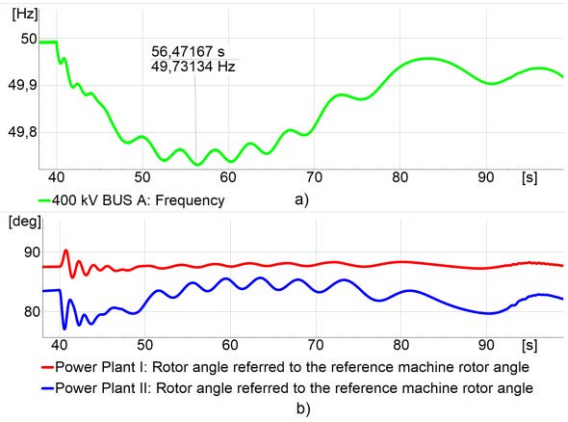

FIGURE 28. a) Frequency variation of power system b) The rotor angle response of generators.

The system frequency begins to decrease until the nadir is 49.73 Hz. When the results of case study-III and IV are compared, the frequency nadir value of case study-IV is lower than case-study-III due to low inertia. On other hand, frequency oscillation is more when the OWPP is integrated into the power system without an interconnection line with other countries. But frequency stability is preserved even if OWPP is at full power without an interconnection line.

5) ADDING NEW LOAD WITH OWPP AT FULL POWER AND WITHOUT INTERCONNECTION LINE TO OTHER COUNTRIES

A new load of 550 MW is added to the power system to examine the frequency stability for OWPP at full power without interconnection lines to other countries at the instant of 40 s. The results of adding the new load are shown in Fig. 29. The frequency variation of the Turkish power system is given in Fig. 29 (a) after adding a new load with OWPP at full power without interconnection. Fig. 29 (b) depicts the rotor angle response of critical generators. When the new load is added, the frequency starts to decrease until the nadir 49.95 Hz and there is an oscillation in frequency and rotor angle of important generators. These oscillations decay and reach the nominal value.

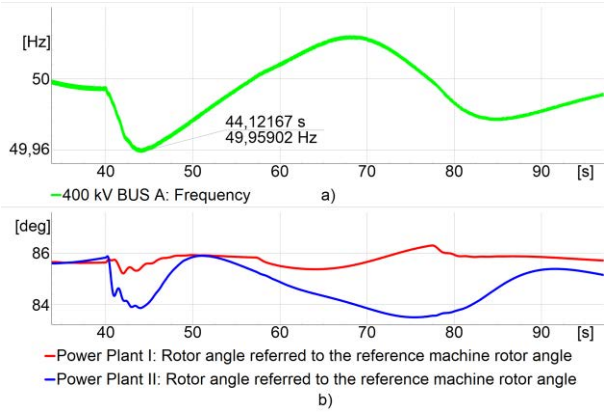

FIGURE 29. a) Frequency variation of power system b) The rotor angle response of generators.

The power system becomes weaker when the interconnection to the UCTE grid is lost. Under such a scenario, the oscillations tend to be higher, however, they decay and stable system operation is achieved.

6) OUTAGE OF PP III WITH OWPP AT FULL POWER AND WITHOUT INTERCONNECTION LINE TO OTHER COUNTRIES USING GRID FORMING CONTROLLER

The virtual synchronous generator (VSG) control structure is shown in Figure 1. In this topology, the converter is normally connected to the grid through a passive inductive-capacitive (LC) filter. R_f, L_f, and C_f are the filter resistance, inductance, and capacitance, respectively, and the interconnection impedance is denoted by R_g and L_g.

The control system includes a traditional current controller and voltage controller as an inner and intermediate loop, respectively. The outer control loops comprise of a conventional reactive and active power droop controller. The active power transferred by the VSG is regulated by the swing equation demonstrated in (2):

$$P_{ref} - P = J\frac{d\omega}{dt} + D(\omega_m - \omega_0) \tag{2}$$

where P_{ref}, P, J, and D are the active power reference, the active power of VSG, the virtual inertia, and the droop coefficient for the active power regulation, respectively, ω_m is the VSG angular frequency, and ω_0 represents the reference grid frequency. Note that if the converter is operated in a grid-connected mode, the VSG control synchronizes to the grid voltage phase angle through the power balance of the

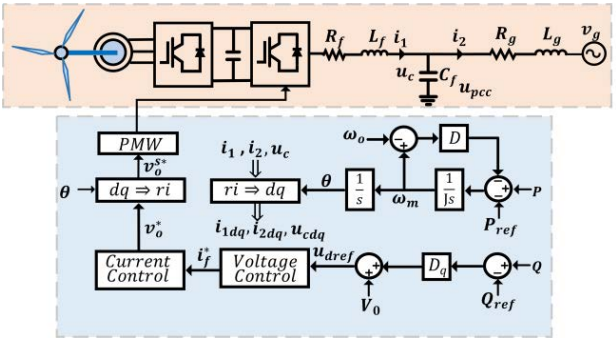

FIGURE 30. VSG-control block diagram.

swing equation. Thus, the normal operation of the VSG does not rely on any grid synchronization method as commonly needed for grid-connected converters.

PP III is disabled to examine the frequency stability for OWPP at full power without interconnection line to the UCTE at the instant of 40 s based on VSG. The results of the outage are shown in Fig. 2. Fig. 2 (a) shows the Turkish power system frequency variation after an outage of a critical conventional power plant with OWPP at full power without interconnection considering VSG. Fig. 2 (b) shows ROCOF considering grid forming and grid following controller.

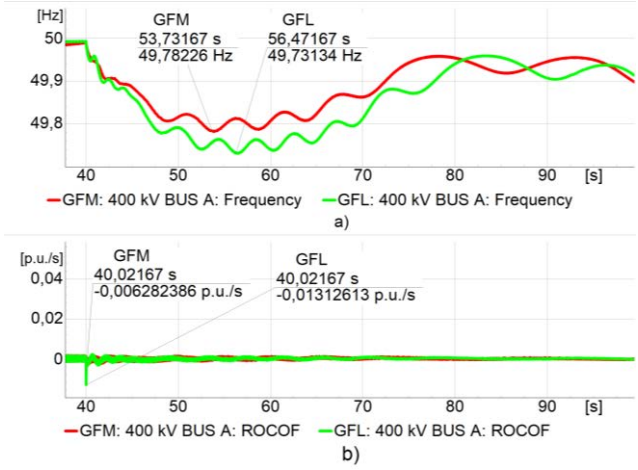

FIGURE 31. a) Frequency variation of power system b) ROCOF.

The results show that the frequency nadir and rate-of-change-of-frequency (ROCOF) are improved when grid forming control is utilized instead of grid feeding control as VSG provides inertia. The frequency nadir value is increased from 49.73 Hz to 47.78 Hz and ROCOF is improved from 0.013 p.u./s to 0.006 p.u./s. Based on the results, when the integration of renewable energy plants increases, the utilization of grid forming controller instead of the conventional controller can be a remarkable option in large-scale renewable power plants in future power systems.

VII. RESULTS AND DISCUSSIONS

The grid compliance analyses of Kıyıköy OWPPs are performed using the grid connection requirements defined in the Turkish grid code. In the grid compliance analyses, reactive power capability, LVRT performance, voltage control performance, and frequency response ability have been analyzed. According to the obtained results, the Kıyıköy OWPPs have satisfied all grid code requirements without any violation.

The static voltage stability analysis is performed using PV and QV curves. The results show that the active power margin for static voltage stability increases from 50970 MW to 51775 MW when the OWPP is connected. Moreover, when the OWPP voltage control is activated, it increases to 51845 MW. When the OWPP is connected, the maximum reactive power level for BUS C increases from 1300 MVAr to 2960 MVAR. Furthermore, when the OWPP voltage control is turned on, it rises to 3200 MVAr.

In dynamic voltage and frequency stability studies, the obtained results show that the grid connection of Kıyıköy OWPP did not create any critical voltage and frequency problems in the Turkish power system. The power system inherently removed voltage and frequency oscillations that appeared in the case studies. A frequency nadir comparison for the different case studies is summarized in Table 7. As can be seen in Table 7, when the penetration level increases, the frequency nadir decreases. The main reason for a lower frequency nadir is that as conventional power plants are replaced by OWPPs, the total inertia of the system decreases.

TABLE 7. Comparison of frequency nadir for different case.

Case Study	Zero Power of OWPP (Hz)	Full Power of OWPP(Hz)
The outage of PP III	49.988	49.987
The outage of PP III without interconnection line	49.76	49.73

VIII. CONCLUSION

The effects of large-scale OWPPs integration on the voltage and frequency stability of Turkey's power system are investigated through various scenarios. Firstly, grid compliance analyses are performed to confirm that the grid code requirements are satisfied by Kıyıköy OWPPs. Static voltage stability analyses are carried out using PV and QV curves to determine the maximum active power margin and minimum reactive power margin. These results show that the current loading level of the grid is greater than the active and reactive power margins. Thus, it was confirmed that there is no static voltage stability problem. Moreover, when the OWPP can provide voltage regulation at the PCC and thus improve the loadability limits.

Different critical fault cases suggested by the TSO have been investigated to analyze the voltage stability of the Turkish power system. It is demonstrated that the OWPP has

TABLE 8. PQ controller parameters.

Symbol	Parameter	Value
K_p	Active power control gain [p.u.]	0,5
T_p	Active power control time constant [s]	0,04
K_q	Reactive power control gain [p.u.]	0,5
T_q	Reactive power control time constant [p.u.]	0,01
X_m	Magnetizing reactance at Pbase [p.u.]	0
deltaU	Voltage dead band [p.u.]	0,1
I_EEG	FRT-mode: 0=acc.TC2007, 1=acc.SDLWindV	1
Tudelay	Voltage support delay [s]	0,01
KdeltaU	Reactive support gain (dyn. Voltage support)	2
i_max	Combined current limit [p.u.]	1
ramp	Active power ramp after FRT [%s]	500
u_max	Max. allowed internal voltage [p.u.]	1,1
X	Coupling reactance [%]	10
id_max	*id* current limit [p.u.]	1
iq_max	*iq* current limit [p.u.]	1

TABLE 9. Current controller parameters.

Symbol	Parameter	Value
K_q	Gain reactive current controller [-]	1
T_q	Integrator time constant reactive current ctrl [s]	0,002
K_d	Gain active current controller [-]	1
T_d	Integrator time constant active current ctrl [s]	0,002
T_m	Current filter time constant	0

a positive impact on fault recovery as the recovery time is reduced from 150 to 80 ms.

The frequency stability analyses were conducted considering the outage of high-power conventional generation plants in the nearby regions. Based on the results, the frequency stability of the Turkish power grid is preserved in the case of the integration of large-scale OWWPs. Moreover, stable system operation is achieved even under weak grid conditions when the transmission lines to Greece and Bulgaria are disconnected.

Effects of grid forming and grid following controllers on the Turkish power system performance have been investigated. In the grid forming controller, frequency stability is improved in terms of frequency nadir and ROCOF.

The simulation results confirm that the Turkish power system does not face any stability problems with the integration of a 1.8 GW renewable power plant. Moreover, when the interconnection lines with neighboring countries are lost, frequency oscillations tend to be higher, however, these oscillations decay, and stable system operation is reached. But, when the penetration level of renewable energy sources (wind, solar) into the grid increases, stability problems may be faced. To solve possible problems, renewable energy plants can be operated in deloading operation, and then they can provide frequency and inertial response to support the power grid. In addition, the frequency oscillations can be reduced by using grid forming controllers such as virtual synchronous generators instead of the grid following controllers. For future work, the effects of grid forming controllers on the power system stability will be investigated in detail. Furthermore, the effectiveness of grid forming and grid following controller utilized in WTs on system stability can be compared.

APPENDIX

Active and reactive power controller parameters, current controller parameters, and active power reduction controller parameters are respectively given in Tables 8-10.

TABLE 10. Parameters of active power reduction controller.

Symbol	Parameter	Value
fUp	Start of Act. Power reduction [Hz]	50,3
fLow	End of Act. Power reduction [Hz]	50,05
PHz	Gradient of Act. Power reduction [%Hz]	40
Tfilter	PT1- Filter time constant [s]	0,1
negGrad	Negative gradient for power change [pu/s]	-0,5
postgrad	Positive gradient for power change [pu/s]	0,5

REFERENCES

[1] D. Henner and REN21. (2017). *Ren21*. [Online]. Available: https://abdn.pure.elsevier.com/en/en/researchoutput/ren21(5d1212f6-d863-45f7-8979-5f68a61e380e).html
[2] Renewable Energy Prospects for the European Union. (2018). *International Renewable Energy Agency (IRENA)*. Accessed: Jul. 29, 2022. [Online]. Available: https://www.irena.org/publications/2018/Feb/Renewable-energy-prospects-for-the-EU
[3] *2030 Climate & Energy Framework*. Accessed: Feb. 9, 2022. [Online]. Available: https://ec.europa.eu/clima/eu-action/climate-strategies-targets/2030-climate-energy-framework_da
[4] *100% Renewable Energy Supply Nordic Energy Research*. Accessed: Feb. 9, 2022. [Online]. Available: https://www.nordicenergy.org/figure/ambitious-climate-targets-and-visions-for-all-nordic-countries/100-renewable-energy-supply/
[5] *Updated Renewable Portfolio Standards Will Lead to More Renewable Electricity Generation Today in Energy U.S. Energy Information Administration (EIA)*. Accessed: Feb. 9, 2022. [Online]. Available: https://www.eia.gov/todayinenergy/detail.php?id=38492
[6] EPDK. (2013). *Electrıcıty Market Network Regulation*. [Online]. Available: https://www.epdk.gov.tr/Detay/Icerik/23-2-3/mevzuat
[7] H. M. Sultan, A. A. Z. Diab, O. N. Kuznetsov, Z. M. Ali, and O. Abdalla, "Evaluation of the impact of high penetration levels of PV power plants on the capacity, frequency and voltage stability of Egypt's unified grid," *Energies*, vol. 12, no. 3, pp. 1–22, 2019, doi: 10.3390/en12030552.
[8] T. Fetouh, T. A. Kawady, H. Shaaban, and A. Elsherif, "Impact of the new Gabl El-Zite wind farm addition on the Egyptian power system stability," in *Proc. 13th Int. Conf. Environ. Electr. Eng. (EEEIC)*, Nov. 2013, pp. 96–103, doi: 10.1109/EEEIC-2.2013.6737890.
[9] K. Kawabe and K. Tanaka, "Impact of dynamic behavior of photovoltaic power generation systems on short-term voltage stability," *IEEE Trans. Power Syst.*, vol. 30, no. 6, pp. 3416–3424, Nov. 2015, doi: 10.1109/TPWRS.2015.2390649.
[10] S. Qutaishat, A. Al-Salaymeh, and H. Obeid, "The dynamic behavior of large scale Safawi PV plant integrated to the national transmission grid of Jordan, particularly 132 kv busbar," in *Proc. 12th Int. Renew. Eng. Conf. (IREC)*, Apr. 2021, pp. 1–6, doi: 10.1109/IREC51415.2021.9427852.
[11] B. B. Adetokun, C. M. Muriithi, and J. O. Ojo, "Voltage stability assessment and enhancement of power grid with increasing wind energy penetration," *Int. J. Electr. Power Energy Syst.*, vol. 120, Sep. 2020, Art. no. 105988, doi: 10.1016/j.ijepes.2020.105988.
[12] M. Hammad and A. Harb, "Static analysis for voltage stability of the northern Jordanian power system," in *Proc. 9th Int. Renew. Energy Congr. (IREC)*, Mar. 2018, pp. 1–5, doi: 10.1109/IREC.2018.8362479.
[13] S. Azzam, E. Feilat, and A. Al-Salaymeh, "Impact of connecting renewable energy plants on the capacity and voltage stability of the national grid of Jordan," in *Proc. 8th Int. Renew. Energy Congr. (IREC)*, Mar. 2017, pp. 1–6, doi: 10.1109/IREC.2017.7926004.
[14] B. Tamimi, C. Canizares, and K. Bhattacharya, "Modeling and performance analysis of large solar photo-voltaic generation on voltage stability and inter-area oscillations," in *Proc. IEEE Power Energy Soc. Gen. Meeting*, Jul. 2011, pp. 5–10, doi: 10.1109/PES.2011.6039797.

[15] M. Ghaffarianfar and A. Hajizadeh, "Voltage stability of low-voltage distribution grid with high penetration of photovoltaic power units," *Energies*, vol. 11, no. 8, p. 1960, Jul. 2018, doi: 10.3390/en11081960.

[16] M. M. S. Khan, "Stability analysis of power system with the penetration of photovoltaic based generation," *Int. J. Energy Power Eng.*, vol. 2, no. 2, p. 84, 2013, doi: 10.11648/j.ijepe.20130202.18.

[17] A. Ameur, K. Loudiyi, and M. Aggour, "Steady state and dynamic analysis of renewable energy integration into the grid using PSS/E software," *Energy Proc.*, vol. 141, pp. 119–125, Dec. 2017, doi: 10.1016/j.egypro.2017.11.023.

[18] S. Mokeke and L. Z. Thamae, "The impact of intermittent renewable energy generators on lesotho national electricity grid," *Electric Power Syst. Res.*, vol. 196, Jul. 2021, Art. no. 107196, doi: 10.1016/j.epsr.2021.107196.

[19] B. Tamimi, C. Canizares, and K. Battacharya, "System stability impact of large-scale and distributed solar photovoltaic generation: The case of Ontario, Canada," *IEEE Trans. Sustain. Energy*, vol. 4, no. 3, pp. 680–688, Jul. 2013, doi: 10.1109/TSTE.2012.2235151.

[20] E. A. Feilat, S. Azzam, and A. Al-Salaymeh, "Impact of large PV and wind power plants on voltage and frequency stability of Jordan's national grid," *Sustain. Cities Soc.*, vol. 36, pp. 257–271, Jan. 2018, doi: 10.1016/j.scs.2017.10.035.

[21] A. S. Saidi, "Impact of large photovoltaic power penetration on the voltage regulation and dynamic performance of the Tunisian power system," *Energy Explor. Exploitation*, vol. 38, no. 5, pp. 1774–1809, Sep. 2020, doi: 10.1177/0144598720940864.

[22] A. Ameur, A. Berrada, K. Loudiyi, and M. Aggour, "Analysis of renewable energy integration into the transmission network," *Electr. J.*, vol. 32, no. 10, Dec. 2019, Art. no. 106676, doi: 10.1016/j.tej.2019.106676.

[23] C. Chompoo-Inwai, W.-J. Lee, P. Fuangfoo, M. Williams, and J. R. Liao, "System impact study for the interconnection of wind generation and utility system," *IEEE Trans. Ind. Appl.*, vol. 41, no. 1, pp. 163–168, Jan. 2005.

[24] *WindFlag*. Accessed: Feb. 9, 2022. [Online]. Available: https://www.windflag.et.aau.dk/

[25] E. Caceoğlu, H. K. Yildiz, E. Oğuz, N. Huvaj, and J. M. Guerrero, "Offshore wind power plant site selection using analytical hierarchy process for northwest Turkey," *Ocean Eng.*, vol. 252, May 2022, Art. no. 111178, doi: 10.1016/j.oceaneng.2022.111178.

[26] *PowerFactory DIgSILENT*. Accessed: Feb. 9, 2022. [Online]. Available: https://www.digsilent.de/en/powerfactory.html

[27] EPDK. (2020). *Electricity Market 2020 Market Development Report*. [Online]. Available: https://www.epdk.gov.tr/Detay/Icerik/3-0-24/elektrikyillik-sektor-raporu

[28] TEIAS. (2020). *Monthly Electricity Production-Consumption Reports*. [Online]. Available: https://www.teias.gov.tr/tr-TR/aylik-elektrik-uretim-tuketim-raporlari

[29] *Political Map of Turkey Nations Online Project*. Accessed: Feb. 9, 2022. [Online]. Available: https://www.nationsonline.org/oneworld/map/turkey-map.htm

[30] Ö. Çelik, Y. Yalman, A. Tan, K. Ç. Bayındır, Ü. Çetinkaya, M. Akdeniz, S. K. Chaudhary, M. Høyer, and J. M. Guerrero, "Grid code requirements—A case study on the assessment for integration of offshore wind power plants in Turkey," *Sustain. Energy Technol. Assessments*, vol. 52, Aug. 2022, Art. no. 102137, doi: 10.1016/j.seta.2022.102137.

[31] T. C. of Denmark. (2020). *Wind Energy Market in Turkey*. [Online]. Available: https://www.danishwindexport.dk/app/uploads/2021/05/TC-Turkey-Wind-Services_20211159.pdf

[32] *Overview of the Turkish Electricity Market*, PWC, London, U.K., 2021, p. 127.

[33] *Global Wind Atlas*. Accessed: Feb. 9, 2022. [Online]. Available: https://globalwindatlas.info/

[34] E. Gaertner, J. Rinker, L. Sethuraman, B. Anderson, F. Zahle, and G. Barter. (2020). *IEA Wind TCP Task 37: Definition of the IEA 15 MW Offshore Reference Wind Turbine*. [Online]. Available: https://github.com/IEAWindTask37/IEA-15-240-RWT

[35] TEIAŞ. *Sayılarla Elektrik Iletimi*. Accessed: Feb. 9, 2022. [Online]. Available: https://www.teias.gov.tr/sayilarla-elektrik-iletimi

[36] DIgSILENT. (2020). *PowerFactory 2020 User Manual*. [Online]. Available: https://www.digsilent.de

[37] P. Kundur, *Power System Stability and Control by Prabha Kundur.Pdf*. New York, NY, USA: McGraw-Hill, 1994, p. 1167.

YUNUS YALMAN was born in Kayseri, Turkey. He received the B.S. degree in electrical engineering from Yildiz Technical University, Istanbul, Turkey, in 2014, and the M.S. degree in electrical and electronics engineering from Ankara Yildirim Beyazit University, Ankara, Turkey, in 2018, where he is currently pursuing the Ph.D. degree with the Department of Electrical and Electronics Engineering. His research interests include renewable energy, transmission systems, and power system stability.

ÖZGÜR ÇELIK received the M.Sc. and Ph.D. degrees from the Department of Electrical and Electronics Engineering, Çukurova University, Adana, Turkey, in 2015 and 2019, respectively. From 2014 to 2021, he was a Research Assistant with the Department of Electrical and Electronics Engineering, Adana Alparslan Türkeş Science and Technology University, where he is currently working as an Assistant Professor with the Department of Energy System Engineering. His current research interests include control of power electronic converters, grid integration of renewable energy systems, and energy efficiency applications.

ADNAN TAN received the M.Sc. and Ph.D. degrees from the Department of Electrical and Electronics Engineering, Çukurova University, Adana, Turkey, in 2011 and 2015, respectively. He has been working as an Assistant Professor with the Electrical and Electronics Engineering Department, Çukurova University, since 2015. His research interests include power electronic converters, utility applications of power electronics, electrical power quality, energy storage systems, and microgrid.

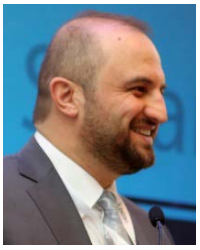

KAMIL ÇAĞATAY BAYINDIR was born in Turkey, in 1973. He received the B.Sc. and M.Sc. degrees in electrical and electronics engineering from Middle East Technical University, Ankara, Turkey, in 1995 and 2000, respectively, and the Ph.D. degree in electrical and electronics engineering from Cukurova University, Adana, in 2006. He was a Research Assistant with Middle East Technical University, from 1997 to 2000. He worked as a Chief Engineer in energy sector for ten years and returned to university, in 2009. From 2009 to 2014, he worked with the Department of Electrical and Electronic Engineering, Faculty of Engineering, Cukurova University. He is currently with Ankara Yıldırım Beyazıt University, Ankara. His research interests include power electronics, electrical power quality, microgrids, and renewable energy applications. He is a member of Turkish TSO Advisory Board and the President of the Association of Digitalization in Energy.

ÜMIT ÇETINKAYA was born in Giresun, Turkey. He received the B.Sc. and M.Sc. degrees, in 2008 and 2017, respectively. He is currently pursuing the Ph.D. degree with Gazi University, Ankara. He is also an Electrical and Electronic Engineer, and he has been working at Transmission System Operator of Turkey, since 2009. His main working areas are power system analysis, grid flexibility, system stability, renewable energy, storage systems, and demand side management. He has articles and notifications within his fields of study. In addition, he has been involved in one national book as the author.

MERDEN YEŞIL was born in Kırsehir, Turkey. He received the B.S. degree in electrical and electronics engineering from Istanbul University, Istanbul, Turkey, in 2007, and the M.S. degree in electrical and electronics engineering from Gazi University, Ankara, Turkey, in 2019, where he is currently pursuing the Ph.D. degree. He also works as a Research and Development Manager at Turkish Electricity Transmission Corporation (TEIAS). His research interests include frequency control improvements in power systems, stability in power systems, electricity markets, electrical power quality, storage systems, and renewable energy applications.

MEVLÜT AKDENIZ received the B.S. degree in electrical engineering from Middle East Technical University, Ankara, in 2005. He has worked for two years as a Junior Researcher at TÜBİTAK, the Scientific and Technological Research Council of Turkey. He is currently a Network Planning Engineer at Turkish Electricity Transmission Corporation, TEİAŞ. He has been working on network expansion, special protection schemes, grid stability, and power plant integration to Turkish transmission grid.

GIBRAN DAVID AGUNDIS TINAJERO (Member, IEEE) received the B.S. degree in mechanical and electrical engineering and the M.Sc. and Ph.D. degrees in electrical engineering from the Universidad Autónoma de San Luis Potosí, San Luis Potosí, Mexico, in 2012, 2014, and 2018, respectively. He is currently working as a Postdoctoral Fellow with the Department of Energy Technology, Aalborg University, Denmark, where he contributes in different renewable-energy related projects. His research interests include modeling, analysis, and control of microgrid clusters, including low voltage (LV) and medium voltage (MV) distribution grids.

SANJAY K. CHAUDHARY (Senior Member, IEEE) received the M.Tech. degree in electrical engineering from IIT Kanpur, Kanpur, India, in 2002, and the Ph.D. degree in electrical engineering from Aalborg University, Aalborg, Denmark, in 2011. He was with ABB Ltd., Bengaluru, India, from 2002 to 2005, and then, he joined the Honeywell Technology Solutions Laboratory, Bengaluru. Since 2011, he has been an Assistant Professor with the Department of Energy Technology, Aalborg University. His current research interests include grid integration of renewable energy, the application of power converters in power systems, high voltage DC transmission, and flexible AC transmission systems.

JOSEP M. GUERRERO (Fellow, IEEE) received the B.S. degree in telecommunications engineering, the M.S. degree in electronics engineering, and the Ph.D. degree in power electronics from the Technical University of Catalonia, Barcelona, in 1977, 2000, and 2003, respectively. Since 2011, he has been a Full Professor with the Department of Energy Technology, Aalborg University, Denmark, where he is responsible for the Microgrid Research Program (www.microgrids.et.aau.dk). He was a Chair Professor with Shandong University, in 2014, a Distinguished Guest Professor with Hunan University, in 2015, and a Guest Professor with the Nanjing University of Posts and Telecommunications. In 2019, he became a Villum Investigator by the Villum Fonden, which supports the Centre for Research on Microgrids, Aalborg University, where being the Founder and the Director. He has published more than 500 journal articles in the fields of microgrids and renewable energy systems, which are cited more than 40 000 times. His research interests include different microgrid aspects, including power electronics, distributed energy-storage systems, hierarchical and cooperative control, energy management systems, smart metering, the Internet of Things for AC/DC microgrid clusters, islanded minigrids, maritime microgrids for electrical ships, vessels, ferries, and seaports. He received the Best Paper Award of the IEEE TRANSACTIONS ON ENERGY CONVERSION, from 2014 to 2015, the Best Paper Prize of IEEE PES, in 2015, and the Best Paper Award of the *Journal of Power Electronics*, in 2016. During six consecutive years, from 2014 to 2019, he was awarded by Clarivate Analytics (Former, Thomson Reuters) as a Highly Cited Researcher. He is an associate editor for a number of IEEE TRANSACTIONS. In 2015, he was elevated as a IEEE Fellow for his contributions on "distributed power systems and microgrids."

BASEEM KHAN (Senior Member, IEEE) received the B.Eng. degree in electrical engineering from Rajiv Gandhi Technological University, Bhopal, India, in 2008, and the M.Tech. and D.Phil. degrees in electrical engineering from the Maulana Azad National Institute of Technology, Bhopal, in 2010 and 2014, respectively. He is currently working as a Faculty Member with Hawassa University, Ethiopia. He has published more than 125 research articles in indexed journals, including IEEE TRANSACTIONS, IEEE ACCESS, *Computers and Electrical Engineering* (Elsevier), *IET Generation, Transmission and Distribution*, *IET Renewable Power Generation*, and *IET Power Electronics*. Further, he has authored and edited books with Wiley, CRC Press, and Elsevier. His research interests include power system restructuring, power system planning, smart grid technologies, meta-heuristic optimization techniques, reliability analysis of renewable energy systems, power quality analysis, and renewable energy integration.